Continuous Supercritical Water Impregnation Method to Prepare Metal Oxide on Activated Carbon Composite Materials

Florentina Maxim *, Elena-Ecaterina Toma, Giuseppe-Stefan Stoian, Cristian Contescu, Irina Atkinson, Christian Ludwig, Speranta Tanasescu

Posted Date: 17 January 2024

doi: 10.20944/preprints202401.1339.v1

Keywords: supercritical water impregnation; continuous flow tubular reactor; supercritical hydrothermal synthesis; metal oxides catalysts; metal oxides sorbents; carbon-based materials

Article

Continuous Supercritical Water Impregnation Method to Prepare Metal Oxide on Activated Carbon Composite Materials

Florentina Maxim [1,*], Elena-Ecaterina Toma [1], Giuseppe-Stefan Stoian [1], Cristian Contescu [2], Irina Atkinson [1], Christian Ludwig [3,4] and Speranta Tanasescu [1]

[1] "Ilie Murgulescu" Institute of Physical Chemistry of the Romanian Academy, Splaiul Independentei 202, 060021 Bucharest, Romania; etoma@icf.ro (E.-E.T.); gstoian@icf.ro (G.-S.S.); irinaatkinson@yahoo.com (I.A.); stanasescu@icf.ro (S.T.)

[2] Oak Ridge National Laboratory, One Bethel Valley Road, Oak Ridge, TN 37831-6087, United States; ccontescu@comcast.net

[3] Paul Scherrer Institute (PSI), ENE LBK CPM, 5232 Villigen PSI, Switzerland; christian.ludwig@psi.ch

[4] École Polytechnique Fédérale de Lausanne (EPFL), ENAC IIE GR-LUD, 1015 Lausanne, Switzerland

* Correspondence: fmaxim@icf.ro

Abstract: Nanomaterials based on metal oxides (Me_xO_y) are employed as catalysts and/or sorbents in processes undergoing conditions in supercritical water (scH_2O), the "green" reaction medium used to obtain energy relevant products. Their properties are greatly affected by the synthesis method used to produce the active Me_xO_y. Moreover, in order to maintain their performance, it is more practical and cost-effective to use supported Me_xO_y nanoparticles. Within this context, the present work deals with the preparation of carbon-supported ZnO and CuO composites by an innovative method based on impregnation under scH_2O conditions. Metal oxides were impregnated on a carbon (C) support using a continuous flow tubular reactor. The results show that impregnation in scH_2O is a promising approach for the preparation of ZnO/C and CuO/C composite materials. This one-step synthesis method, in a continuous flow, uses neither seed layer nor mineralizer, and it needs substantially lower preparation times than the conventional impregnation methods.

Keywords: supercritical water impregnation; continuous flow tubular reactor; supercritical hydrothermal synthesis; metal oxides catalysts; metal oxides sorbents; carbon-based materials

1. Introduction

The supercritical fluid is the state above the critical temperature (T_{cr}) and critical pressure (p_{cr}) in the pressure-temperature phase diagram [1]. In the van der Waals theory of criticality, the critical point is the end of the liquid–gas equilibrium curve, the point in which liquid and gas reach the same density, the critical density (ρ_{cr}) [2]. For water, the corresponding values at the critical point are T_{cr} = 647 K, p_{cr} = 221 bar and ρ_{cr} = 322 kg m^{-3}.

There was a vivid debate on whether there is a liquid–gas phase change associated to the fluid properties variations in the region near the critical point, as no macroscopically visible interface between liquid and gas appears in this region. Therefore, in the text books the supercritical state of a fluid is still presented as a homogeneous phase above the critical point [3]. However, since 2010 it was demonstrated both theoretically and experimentally [4–6], and now it is accepted that the supercritical state of a fluid can be divided into a gas-like (GL) region and a liquid-like (LL) regime by the transitional line, known as Widom line [7–9], anticipating the phase separation and the coexistence that is found below the critical point [10].

The motivation for our work is mainly related to the technological applications of scH_2O. For instance, water and waste water treatments can be done by oxidation in scH_2O [11,12], and gas fuel, such H_2 or CH_4, can be obtained from wet biomass by gasification [13,14]. The main advantage of scH_2O technologies is the efficiency, which resides in the fact that complete conversion or total removal of organic pollutant is achieved very fast, sometimes after only few minutes [15]. Moreover,

 doi:10.20944/preprints202401.1339.v1

using scH_2O, technically difficult feedstocks can be treated in effective way, with high selectivity for valuable compounds, while the reactions products are harmless [16]. However, the disadvantages of scH_2O technologies are the high operation costs resulting from high temperature and pressure working conditions and the associated issues related with salts deposition. A solution to these problems can be the use of functional materials [17], such as catalysts, that could decrease the process temperature and lead to energy savings. The sorbent materials can adsorb heteroatoms, such as sulfur or chlorine, which helps overcoming issues related to salts precipitation and catalysts poisoning. Metal oxides are good candidates as catalysts or sorbents in scH_2O [17–19]. Their functional properties, such as their activity, selectivity and stability under supercritical conditions, might be greatly affected by the synthesis method. Among various preparation methods, the hydrothermal synthesis in scH_2O has the following advantages: high reactions rate, one-step production of well-defined Me_xO_y with controlled size and shape, and reduced alkaline concentration for the crystal growth [20,21]. In addition, running the hydrothermal synthesis in a flow reaction system is more advantageous over using batch reactors due to the possibility to include engineered mixers for the scH_2O and the metal salt precursors [22]. Moreover, in flow reaction systems the density of water can be varied by controlling the temperature and pressure during the reaction.

Considering that it is very important to maintain the performance of the metal oxides as catalysts or sorbents under scH_2O conditions, it is efficient and cost-effective to use supported Me_xO_y nanoparticles, with the advantages of enhanced mechanical and thermal stability, and facile regeneration and reuse. The usual procedure for preparation of composite materials is impregnation followed by drying to obtain the final composite. The loading (amount of metal oxide which determines its efficiency) on the support and the dispersion (concentration profile) within the support pores depend significantly on the impregnation and drying conditions [23]. It is to note that by conventional impregnation methods, such as wet impregnation and pore volume impregnation [24], redistribution of active metal oxides can occur during drying, which in turn lowers the catalytic/sorption capacity. The supercritical water impregnation method in a batch reactor was developed in order to obtain highly dispersed metal oxides on porous support [25]. Moreover, the method simplifies the process of impregnation due to the fact that post-treatments, such as calcining and drying, are not needed [26] and therefore avoids the agglomeration and/or the redistribution of the active nanoparticles within the support.

The present work is focused on development of a continuous flow supercritical water impregnation method for preparation of zinc oxide and copper oxide nanoparticles on carbon support, which are composite materials with specific functionalities for separation processes in scH_2O.

2. Materials and Methods

$Zn(NO_3)_2 \cdot 6H_2O$ and $Cu(NO_3)_2 \cdot 3H_2O$ of analytical purity from Sigma Aldrich were used as precursors. Aqueous solutions of different concentrations, namely, 0.0041 M, 0.0082 M and 0.0164 M, were prepared in ultrapure, degassed water. Porous materials based on carbon were used as a support for the impregnation of the metal oxides. The carbonaceous porous material samples have a graphitic, monolithic structure and are constituted by activated carbon fibers with an average diameter in the micrometric scale (10-20 μm) [8]. The support has the following characteristics: specific surface area of approx. 1100 $m^2\ g^{-1}$ and total pore volume of approx. 0.6 $cm^3\ g^{-1}$ measured by N_2 adsorption at 77 K, and water absorption capacity of 165%.

Metal oxides were impregnated using the continuous flow tubular reactor of the NISA equipment (*Neutron Imaging Supercritical-water Analysis*) described in [8]. The main component of NISA is the continuous flow tubular reactor, equipped with an embedded preheater, and an aluminum block heater. The fluid is fed in the reactor in the upwards direction by high-pressure liquid chromatography pumps. In the setup, the pressure is built and controlled with the back pressure regulator. The operating parameters, such as temperature, pressure, water flow rate, and mass balance are controlled and monitored on-line, and the values are recorded every 10 seconds [8]. Three synthesis parameters were studied to understand their influence on the composite's

 doi:10.20944/preprints202401.1339.v1

formulation in terms of crystallinity, size and morphology, as well as the loading and concentration profile of the active element on the support. They were *i*) the impregnation temperature chosen to provide scH_2O densities corresponding either to LL or to GL phases of water [9], *ii*) the flow rate determining both the residence time and the contact time between the metal precursor solution and the C support surface, and *iii*) the concentration of the metal nitrate aqueous solution used as precursor.

Each experimental run started by loading the reactor with ~ 0.2 g of carbon support, followed by filling the system with water, preheating at 573 K, and application of a constant pressure of 250 bar to reach supercritical conditions. When water inside the reactor reached the temperature of interest for impregnation, metal precursor solution was fed in at flow rates of 2.5 mL min^{-1}, 5 mL min^{-1} or 7.5 mL min^{-1}, and the impregnation was performed at steady-state conditions for 1 h. The mass of the metal precursor solution was recorded for each experiment, and the amount of metal available for deposition on the carbon support was calculated this way. The impregnation temperature was either 648 K or 668 K. These temperatures were chosen to be 10 K lower and higher, respectively, than the transition temperature between the LL and GL phases of scH_2O at the pressure of 250 bar [9]. The sample index contains the starting metal ion/the molar concentration of the aqueous nitrate solution (mol L^{-1}) / the fluid flow rate (mL min^{-1}) / the synthesis temperature (K). For example, the sample obtained from 0.0041 M zinc nitrate at 5 mL min^{-1} flow rate and 668 K was indexed as Zn^{2+}/0.0041 M/5 mL min^{-1}/668 K.

The structural analysis of the as obtained composite materials was conducted by X-ray diffraction (XRD) at room temperature. The XRD patterns were recorded using Rigaku's Ultima IV diffractometer in parallel beam geometry, using Cu Kα radiation (λ = 1.5406 Å), operating at 40 kV and 30 mA. The signals were collected from 10º to 80º with a step size of 0.02º, and a scan speed of 2º min^{-1}. Phase identification was performed using Rigaku's PDXL software, connected to ICDD PDF-2 database.

The infrared spectroscopy (FTIR) was performed using a NICOLET IS10 spectrometer (Thermo Fisher, Eindhoven, Netherlands). The measurements were done at room temperature using the total attenuated reflection module with scans between 500 and 4000 cm^{-1}. The peak locations and intensities were determined with the Omnic software (Nicolet Instrumentations Inc., Madison, WI, USA).

The morphology was analyzed by scanning electron microscopy (SEM) with a FEI Quanta 3D FEG microscope operated at 5 kV acceleration voltages and at 10 mm working distance using the secondary electrons detector. The transmission electron microscopy (TEM) characterization of the composite materials was performed on a Hitachi HD-2700 Scanning Transmission Electron Microscope (STEM) at 200 kV accelerating voltage with a crystal lattice resolution of 0.144 nm under ideal conditions. Chemical composition analysis was performed with the same equipment using the EDS short-time elemental mapping module. For the TEM analysis the samples obtained by impregnation at scH_2O conditions were crushed and dispersed in ethanol. A drop of the resulting suspension was then deposited on a Cu grid containing a holey carbon thin film.

3. Results

3.1. Effect of the impregnation temperature

Figure 1 presents the XRD patterns of the samples obtained from Zn^{2+} and Cu^{2+} precursors, at two different impregnation temperatures, 648 K and 668 K, respectively. The XRD analysis revealed that ZnO with hexagonal structure is formed at both temperatures (Figure 1a). It is important to notice that the ZnO XRD peaks intensity were smaller as the reaction temperature increased. This is different when starting from Cu precursor, where formation of copper oxides was revealed by XRD only at impregnation temperatures above the Widom line (668 K).

Preprints (www.preprints.org) | NOT PEER-REVIEWED | Posted: 17 January 2024 doi:10.20944/preprints202401.1339.v1

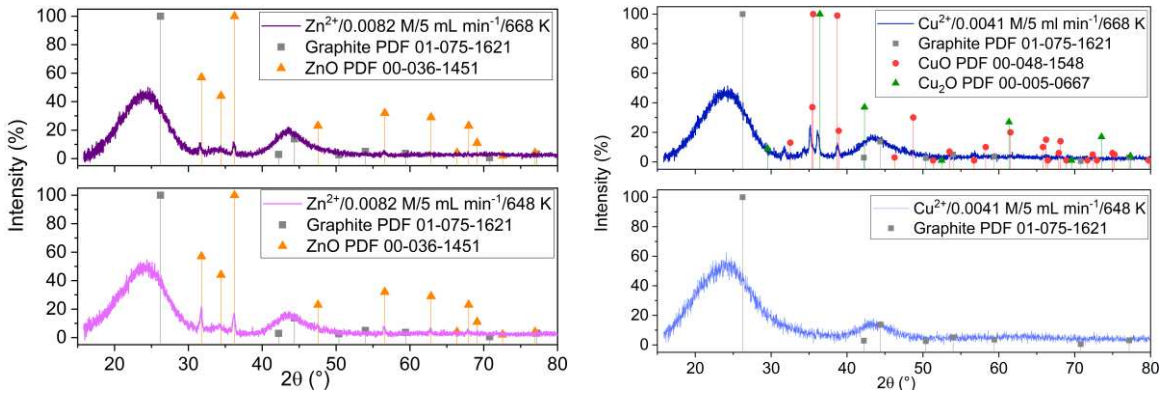

(**a**) (**b**)

Figure 1. XRD patterns of the samples obtained at two different impregnation temperatures and starting from (**a**) zinc and (**b**) copper precursors.

Figure 2 shows FTIR spectra of ZnO/C and CuO/C type composite materials obtained at 668 K, and for comparison, the spectrum of the initial carbon support. The three spectra are similar at wave numbers up to 1200 cm^{-1}. The spectral bands observed in the region 3600-3100 cm^{-1} are attributed to the O-H bonds in the water molecule. Also, OH groups were confirmed by discrete absorption bands around 1387-1405 cm^{-1} [27]. The bands in the 2600–1900 cm^{-1} region correspond to C=C stretching vibrations of numerous sp^2 structures that enrich the carbon structure [28]. The presence of C=O bonds is indicated by the spectral bands in the 1500-1400 cm^{-1} range. The bands specific to metal-oxygen bonds are observed in the fingerprint region between 1200 and 700 cm^{-1} [29]. Moreover, characteristic bands of the Cu-O bonds were observed in the region of 550-600 cm^{-1} [30,31].

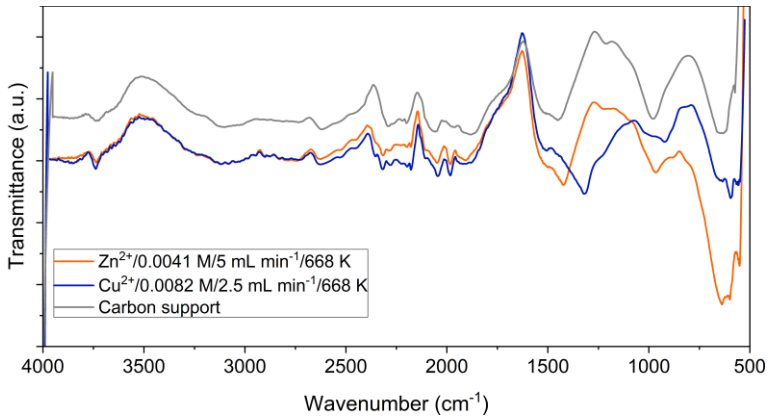

Figure 2. FTIR spectra of ZnO/C and CuO/C composite materials; the spectrum of the carbon support is presented for comparison.

We analyzed the effect of the impregnation temperature by SEM, and the results are presented in Figure 3. Note that, starting from either Zn^{2+} or Cu^{2+} precursors, Me_xO_y particles with 1D rod-like morphology and diameter within the μm scale were formed at 648 K; this type of particles appears to be formed separate from the carbon fibers surface (Figures 3a-3d). SEM analysis of samples obtained at the impregnation temperature of 668 K (Figures 3e-3h), reveals carbon fibers covered by Me_xO_y nanoparticles on the surface along with isolated regions containing the 1D Me_xO_y particles. Based on this observation, impregnation/deposition of metal oxide structures on the carbon surface was further performed at this temperature.

Preprints (www.preprints.org) | NOT PEER-REVIEWED | Posted: 17 January 2024 doi:10.20944/preprints202401.1339.v1

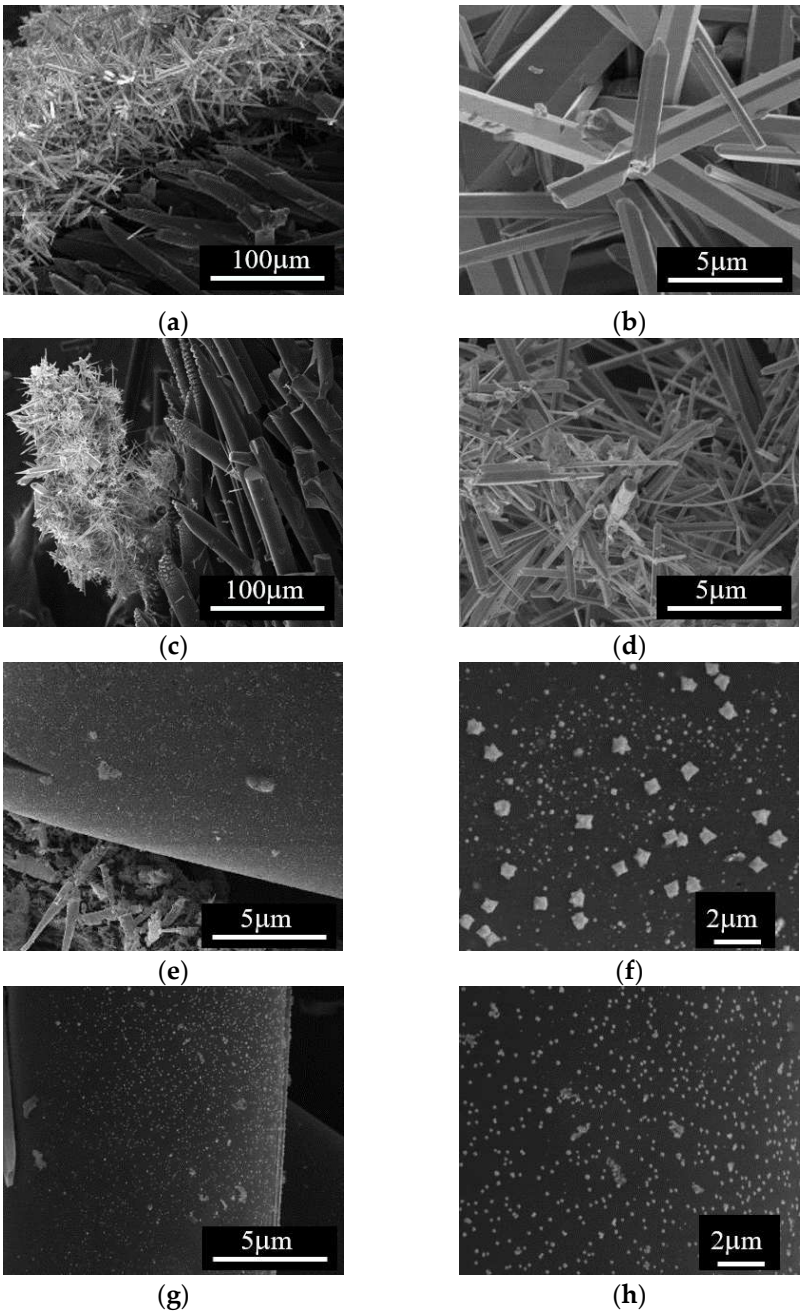

Figure 3. SEM images of the samples obtained at different impregnation temperatures: (**a**), (**b**), (**c**) and (**d**) at 648 K; (**e**), (**f**), (**g**) and (**h**) at 668 K, starting from (**a**), (**b**), (**e**) and (**f**) Zn^{2+} and (**c**), (**d**), (**g**), and (**h**) Cu^{2+} precursors; right side SEM images are higher magnification of the images presented on the left side.

Figure 4 shows results of TEM characterization and chemical composition analysis by EDS for the ZnO/C type material obtained at 668 K, with 5 mL min^{-1} flow rate, and 0.0041 M zinc concentration in the precursor solution. The TEM images (Figures 4a and 4b) reveal the formation of small crystalline particles of approx. 50 nm in size and the EDS maps presented in Figures 4c-4f confirm that these nanoparticles are ZnO on C support.

Preprints (www.preprints.org) | NOT PEER-REVIEWED | Posted: 17 January 2024 doi:10.20944/preprints202401.1339.v1

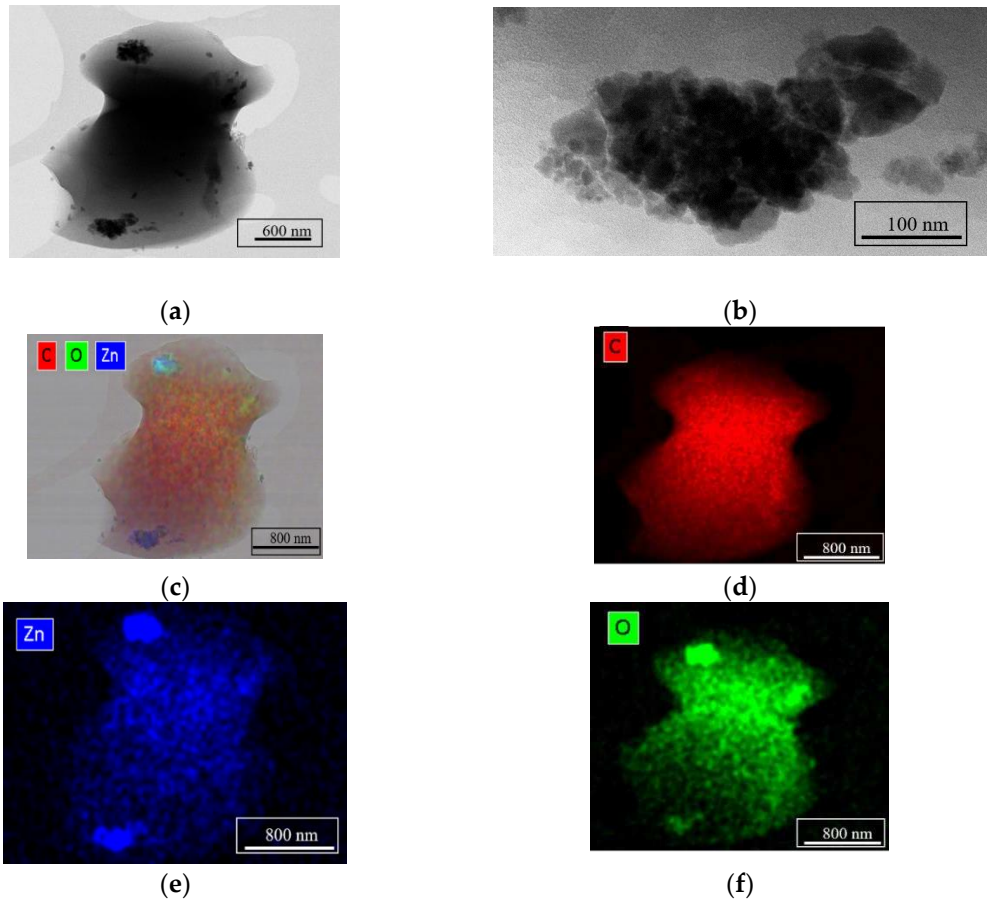

Figure 4. TEM characterization of the sample Zn^{2+}/0.0041 M/5 mL min^{-1}/668 K: (**a**) and (**b**) STEM images; (**c**), (**d**), (**e**) and (**f**) the EDS maps confirming the formation of ZnO nanoparticles on C support.

3.2. Effect of the fluid flow rate

Figure 5 presents the XRD analysis of the samples obtained from Zn^{2+} (Figure 5a) and Cu^{2+} (Figure 5b) precursors with two different flow rates of the reactant mixture during the impregnation (2.5 mL min^{-1} and 5mL min^{-1}, respectively). It is to notice that, increasing the flow rate allows the formation of more crystalline ZnO (Figure 5a) and the formation of CuO (Figure 5b). At low flow rate instead, Cu_2O is predominately formed indicating the influence of the redox environment related to the higher rate of mixing.

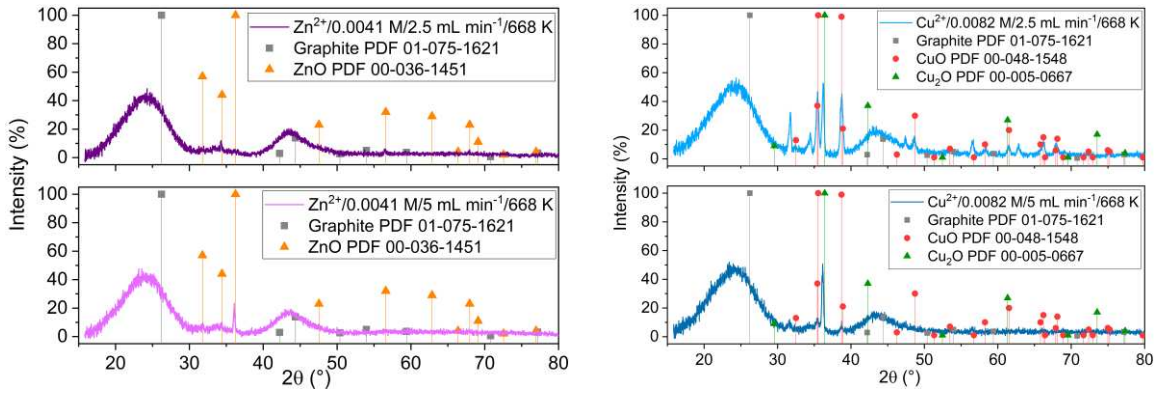

Figure 5. XRD patterns of the samples obtained at 668 K, different flow rates and starting from (**a**) Zn^{2+} and (**b**) Cu^{2+} precursors.

Preprints (www.preprints.org) | NOT PEER-REVIEWED | Posted: 17 January 2024 doi:10.20944/preprints202401.1339.v1

The effect of the flow rate on the impregnation procedure is more evident from SEM analysis of ZnO/C composite materials presented in Figure 6. There are 1D particles attached to the carbon fibers at both flow rates (Figures 6a, 6b, 6e and 6f), however, at low flow rate, the surface of the carbon fibers is covered by hexagonal shaped nanoparticles of different sizes (Figures 6c and 6d), while at higher flow rate there are carbon fibers homogenously covered with Me_xO_y crystalline cuboid-shaped nanoparticles of about 60 nm in size (Figures 6g and 6h).

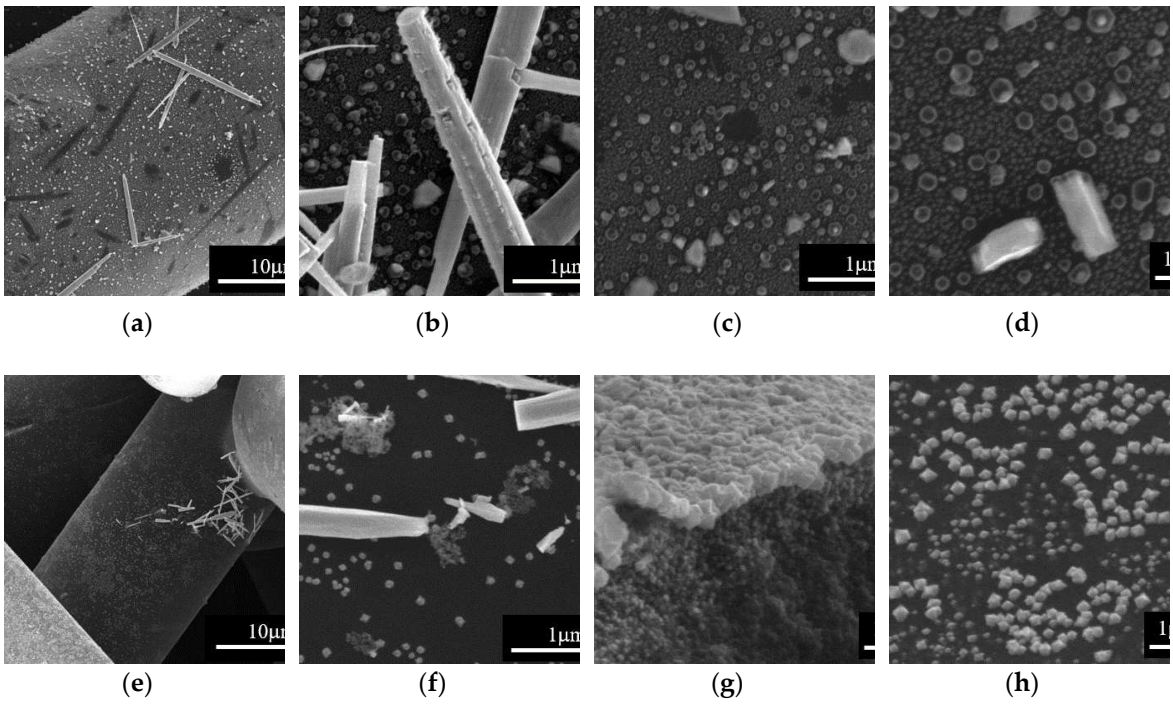

Figure 6. SEM analysis of the ZnO/C samples obtained starting from $[Zn^{2+}] = 0.0041$ M, by impregnation at 668 K and two different flow rates of the reactant mixture: (**a**), (**b**), (**c**), and (**d**) at 2.5 mL min^{-1}; (**e**), (**f**), (**g**), and (**h**) at 5 mL min^{-1}.

3.3. Effect of the metal ions concentration in the aqueous precursor solution

The XRD patterns of ZnO/C composite materials obtained from different concentrations of precursor solution are presented in Figure 7a. Note that hexagonal ZnO structures were formed at all initial Zn^{2+} concentrations, whereas high crystallinity ZnO was obtained only by increasing the starting amount of zinc ions (inset in Figure 7a). The XRD results of the samples obtained from Cu^{2+} precursor, with different initial concentrations are presented in Figure 7b. The important observation from the analysis of XRD patterns of these samples is that decreasing the Cu^{2+} concentration might promote the formation of CuO. However, the inset in Figure 7b shows that the corresponding diffraction peaks of Cu_2O structure are shifted towards lower 2θ angles compared to the reference. Moreover, unidentified diffraction peaks appear in the XRD patterns of these samples. Surprisingly, no copper oxides formation at high concentration was revealed by XRD.

Preprints (www.preprints.org) | NOT PEER-REVIEWED | Posted: 17 January 2024 doi:10.20944/preprints202401.1339.v1

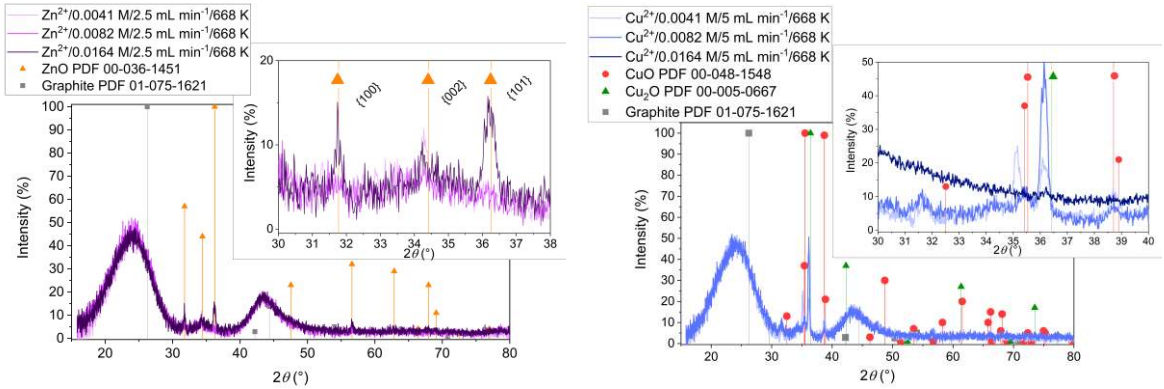

(**a**) (**b**)

Figure 7. XRD patterns of the samples obtained from (**a**) Zn^{2+} and (**b**) Cu^{2+} and different metal ion concentrations in the precursor solutions.

By SEM, the effect of the initial cation concentration on the impregnation of Me_xO_y is more evident for the ZnO/C type samples, as presented in Figure 8. First to note is that zinc oxide nanoparticles were deposited on the carbon fibers' surface at all starting concentration of Zn^{2+} in the precursor solution (Figures 8a, 8d and 8f). Secondly, at low concentration, we noticed that ZnO cover more homogeneously the carbon fibers, while increasing the Zn concentration leads to the increasing in the particles' dimensions from around 60 nm (Figure 8b) to 80 nm (Figure 8e), and finally to over 200 nm (Figure 8g). Finally, it is to note the flower-like morphology of the ZnO nanoparticles (Figures 8c and 8h).

The SEM analysis of the sample obtained at 668 K with the low Cu^{2+} concentration and low flow rate of the precursor solution, showed formation of large 1D particles together with nanoparticles uniformly covering large areas of the carbon surface. Figure 9 presents this result and shows morphological details at different magnifications, of copper oxides nanoparticles formed under the above-mentioned conditions.

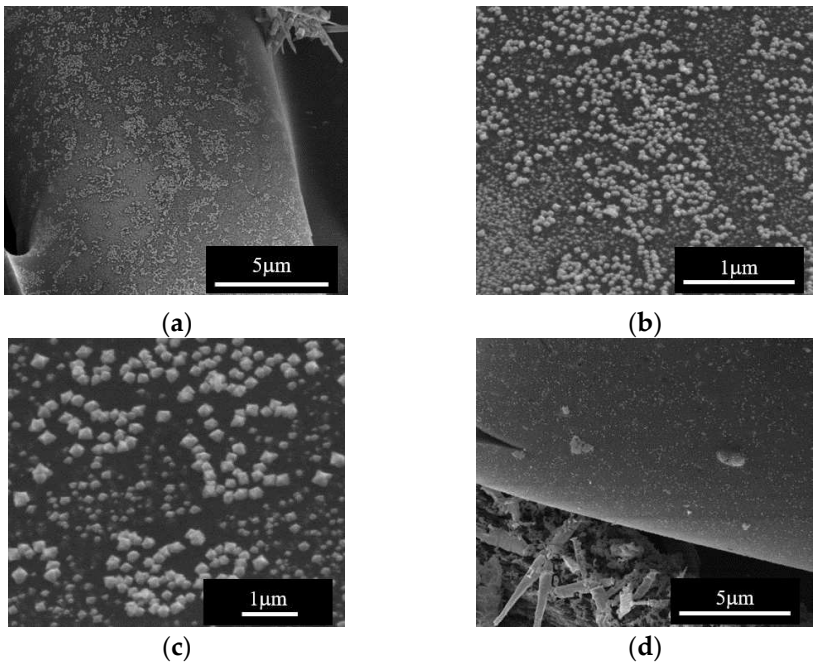

(**a**) (**b**)

(**c**) (**d**)

Preprints (www.preprints.org) | NOT PEER-REVIEWED | Posted: 17 January 2024 doi:10.20944/preprints202401.1339.v1

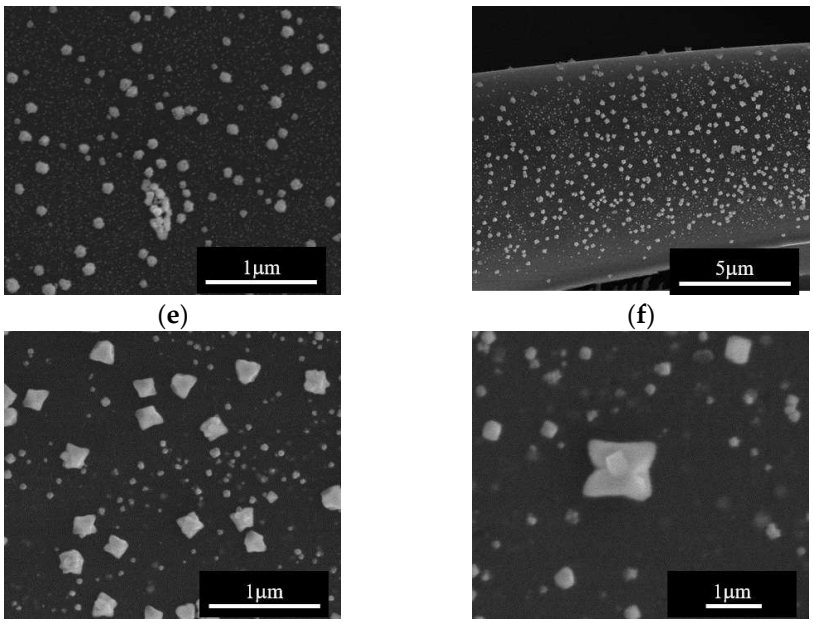

(**e**) (**f**)

(**g**) (**h**)

Figure 8. SEM images of samples obtained at different concentrations of Zn^{2+} in the precursor solution: (**a**), (**b**), and (**c**) for Zn^{2+}/0.0041 M/5 mL min^{-1}/668 K; (**d**), and (**e**) for Zn^{2+}/0.0082 M/5 mL min^{-1}/668 K; (**f**), (**g**), and (**h**) for Zn^{2+}/0.0164 M/5 mL min^{-1}/668 K.

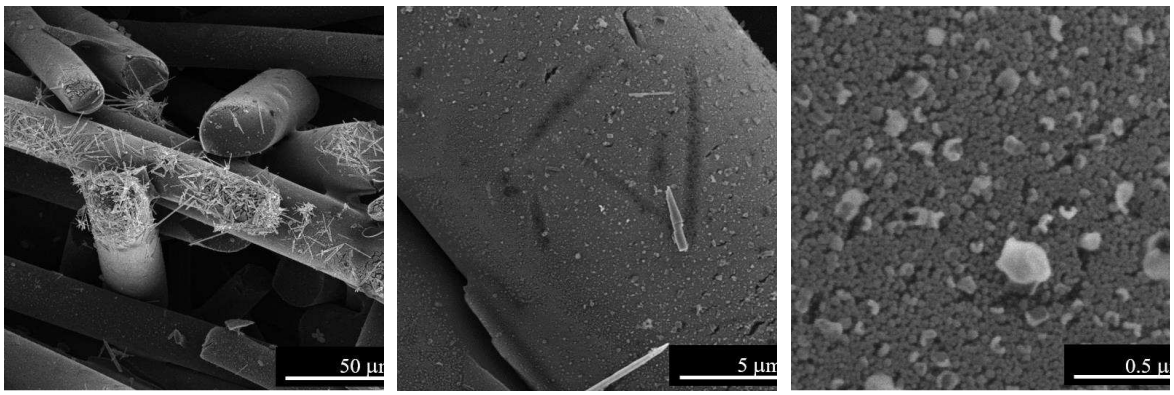

(**a**) (**b**) (**c**)

Figure 9. SEM analysis of sample Cu^{2+}/0.0041 M/2.5 mL min^{-1}/668 K showing microstructural and morphological details of the surface of the CuO/C composite material, at different magnifications.

4. Discussion

The above presented results show that zinc oxide and copper oxides are formed under scH_2O conditions, and that the 668 K impregnation temperature is optimum for the deposition of Me_xO_y nanoparticles on the carbon fibers support (Figures 1, 2, 3, 4). This temperature and low flow rates of the metal precursor solution favor the formation of CuO (Figure 5), while high flow rate of Zn^{2+} solution allows homogenous deposition of ZnO nanoparticles on carbon fibers' surface (Figure 6). The metal ion concentration in the starting solution does not have significant influence on the formation of Me_xO_y structures (Figure 7). However, increasing the Zn^{2+} concentration resulted in the increasing size of the flower-like ZnO nanoparticles impregnated on the carbon fibers (Figure 8). Instead, copper oxides nanoparticles are more homogenously impregnated on the support fibers at low concentration of Cu^{2+} in the precursor solution (Figure 9).

The related hydrothermal reactions leading to the formation of metal oxides from nitrates correspond to hydrolysis of metal ions and dehydration of the corresponding hydroxides, according to the reactions below:

 doi:10.20944/preprints202401.1339.v1

$$\text{Hydrolysis: } Me(NO_3)_x + xH_2O \rightarrow Me(OH)_x + xHNO_3 \quad (1)$$

$$\text{Dehydration: } Me(OH)_x \rightarrow MeO_{x/2} + x/2\ H_2O \quad (2)$$

In this homogeneous phase mechanism, water acts as both reactant and solvent and its properties variation, like density and dielectric constant, affects significantly the rate of these reactions [21].

Based on neutron imaging measurements, Maxim *et al.* obtained the water phase diagram in the supercritical region and confirmed the position of the Widom line that separates the LL and GL regimes of the scH_2O [9]. At 250 bar the water temperature of 648 K corresponds to the LL densities with values around 500 kg m^{-3}, while at 668 K water is in the GL state, with density around 150 kg m^{-3}. Moreover, the dielectric constant of water drops from values around 10 to below 5 when increasing the temperature across the Widom line [32]. Water properties variation explains the effect of synthesis temperature on the formation of Me_xO_y during impregnation on C fibers. It is known that, on increasing the temperature under supercritical conditions, the hydrolysis rate of metal salts precursor substantially increases with the decreasing of water dielectric constant, while the dehydration equilibrium shifts towards oxides [21]. This is also in agreement with the study by Ludwig and Casey [33] who concluded, that hydrolyzed cations are more reactive than non-hydrolyzed cations. Hydrolyzed species may, therefore, favor the formation of Me_xO_y structures and play a role as relevant precursors under the scH_2O conditions as presented in this study. However, further studies are needed to elucidate the details of the Me_xO_y formation mechanism at scH_2O conditions.

Interestingly, carbon fibers impregnation with Me_xO_y nanoparticles was observed only at synthesis temperatures corresponding to the GL phase of scH_2O. In the GL phase the dielectric constant of scH_2O is two times lower than in the LL state. Consequently, the metal salts hydrolysis reaction rate increases substantially and formation of nitric acid is faster under GL conditions than in the LL regime. Surface carbon oxidation by NO_3^- ions may possibly initiate a second, heterogeneous mechanism for copper oxide deposition. Oxidation introduces oxygen-containing surface groups, (carboxyls, phenols) which increase the hydrophilic character of carbon surface and likely enhance cations adsorption of hydrated cations [34]. Both carboxylic and phenolic groups act as ligands for Cu^{2+} and Zn^{2+} ions, and may displace water from the aqueous ion. [35] The higher difficulty of obtaining copper oxides compared with zinc oxide reported above may originate in the higher stability of copper complexes with oxygenated functional groups on carbon surface. Indeed, Cu^{2+} (d^9) complexes on carbon surface should be more stable than Zn^{2+} (d^{10}) analogues [36,37] for reasons that depend on ion size differences and a possible Jahn-Teller symmetry deformation only for Cu^{2+}.

The *in-situ* neutron imaging measurements reported by Maxim *et al.* [8] help to understand that the carbon monolith used as support for impregnation is acting as a static mixer [38] which allows visualization of different hydrodynamic regimes inside the monolith in the neutron radiographies of the scH_2O reactor [8]. Therefore, it is expected that the reactant mixture flow rate influences the mixing rate within the monolith support and the residence time of metal precursors on the fibers' surface. It is known that, in order to obtain well-defined Me_xO_y nanoparticles in terms of size, morphology and structure, the mixing rate of scH_2O with the metal precursor solution should be high compared to the formation reaction rate [39,40]. Zinc and copper oxides are formed under the studied scH_2O conditions independently on the flow rate, however the SEM analysis confirmed that there is a nucleation and growth mechanism difference when changing the flow rate. Moreover, the concentration of the metal ions in the precursor solution might influence the growth direction and the aspect ratio of the Me_xO_y nanoparticles, results that are in agreement with previous reports, especially for the ZnO synthesis in scH_2O [41,42].

5. Conclusions

Under isobaric supercritical conditions, increasing the synthesis temperature to values at which scH_2O is in the GL phase favors impregnation of metal oxides on activated carbon fibers monolithic supports. Uniform impregnation of support fibers with ZnO crystalline nanoparticles of hexagonal

symmetry, cubic morphology and ~60 nm in size was obtained at 250 bar and a reaction temperature of 668 K. Under the same temperature and pressure conditions, impregnation of CuO on the same type of support is favored when starting from low concentrations of Cu^{2+} in the aqueous precursor solution and at low flow rates of the precursor solution through the reactor. Those conditions determine the contact time between the metal precursor and the surface of the carbon support. Crystalline nanoparticles of cupric oxide, of monoclinic symmetry and cubic morphology, with dimensions of 50 nm, uniformly cover the carbon fibers.

The results show that hydrothermal impregnation in scH_2O is a promising method for the preparation, in continuous flow, of Me_xO_y/C composite materials. The method described here has the advantages that it can be performed in a single synthesis step, without a seed layer and without a mineralizer, and at substantially lower preparation times than conventional impregnation methods.

Author Contributions: Conceptualization, F.M.; methodology, F.M., E.T., G.S.; data curation, E.T., G.S., I.A., and M.F.; writing—original draft preparation, F.M., C.C., C.L.; writing—review and editing, F.M., C.C., C.L., and S.T.; All authors have read and agreed to the published version of the manuscript.

Funding: This work was supported by a grant of the Romanian Ministry of Research, Innovation and Digitization, CNCS/CCCDI – UEFISCDI, project number PN-III-P4-ID-PCE-2020-1241 (acronym APASUPER), within PNCDI III.

Data Availability Statement: Not applicable.

Acknowledgments: The work with the NISA setup at "Ilie Murgulescu" Institute of Physical Chemistry is possible due to the Research Collaboration Agreement between the Romanian Institution and Paul Scherrer Institute, Switzerland. Eng. Cristian Iacob from Computer Power SRL, Romania is truly acknowledged for the technical support. Dr. Florina Teodorescu from Institute of Physical Chemistry, Romania is acknowledged for valuable discussions. The authors are thankful to Marta Ferro from University of Aveiro, Portugal for the TEM characterization.

Conflicts of Interest: The authors declare no conflict of interest.

References

1. Atkins, P.; de Paula, J. *Physical Chemistry*; 8th ed.; W. H. Freeman and Company: New York, 2006;
2. Peng, D.Y.; Robinson, D.B. A New Two-Constant Equation of State. *Ind. Eng. Chem. Fundam.* **1976**, *15*, 59–64, doi:10.1021/i160057a011.
3. Wang, S.; Xu, D.; Guo, Y.; Tang, X.; Wang, Y.; Zhang, J.; Ma, H.; Qian, L.; Li, Y. *Supercritical Water Processing Technologies for Environment, Energy and Nanomaterial Applications*; Springer Singapore: Singapore, 2020; ISBN 978-981-13-9325-9.
4. McMillan, P.F.; Stanley, H.E. Going supercritical. *Nat. Phys.* **2010**, *6*, 479–480, doi:10.1038/nphys1711.
5. Simeoni, G.G.; Bryk, T.; Gorelli, F.A.; Krisch, M.; Ruocco, G.; Santoro, M.; Scopigno, T. The Widom line as the crossover between liquid-like and gas-like behaviour in supercritical fluids. *Nat. Phys.* **2010**, *6*, 503–507, doi:10.1038/nphys1683.
6. Simeski, F.; Ihme, M. Supercritical fluids behave as complex networks. *Nat. Commun.* **2023**, *14*, 1996, doi:10.1038/s41467-023-37645-z.
7. Banuti, D.T. Crossing the Widom-line - Supercritical pseudo-boiling. *J. Supercrit. Fluids* **2015**, *98*, 12–16, doi:10.1016/j.supflu.2014.12.019.
8. Maxim, F.; Contescu, C.; Boillat, P.; Niceno, B.; Karalis, K.; Testino, A.; Ludwig, C. Visualization of supercritical water pseudo-boiling at Widom line crossover. *Nat. Commun.* **2019**, *10*, 4114, doi:10.1038/s41467-019-12117-5.
9. Maxim, F.; Karalis, K.; Boillat, P.; Banuti, D.T.; Marquez Damian, J.I.; Niceno, B.; Ludwig, C. Thermodynamics and Dynamics of Supercritical Water Pseudo-Boiling. *Adv. Sci.* **2021**, *8*, 2002312, doi:10.1002/advs.202002312.

10. Banuti, D.T.; Raju, M.; Ihme, M. Similarity law for Widom lines and coexistence lines. *Phys. Rev. E* **2017**, *95*, doi:10.1103/physreve.95.052120.
11. Zhang, S.; Zhang, Z.; Zhao, R.; Gu, J.; Liu, J.; Örmeci, B.; Zhang, J. A Review of Challenges and Recent Progress in Supercritical Water Oxidation of Wastewater. *Chem. Eng. Commun.* **2017**, *204*, 265–282, doi:10.1080/00986445.2016.1262359.
12. de Souza, G.B.M.; Pereira, M.B.; Mourão, L.C.; dos Santos, M.P.; de Oliveira, J.A.; Garde, I.A.A.; Alonso, C.G.; Jegatheesan, V.; Cardozo-Filho, L. Supercritical water technology: an emerging treatment process for contaminated wastewaters and sludge. *Rev. Environ. Sci. Bio/Technology* **2022**, *21*, 75–104, doi:10.1007/s11157-021-09601-0.
13. Okolie, J.A.; Rana, R.; Nanda, S.; Dalai, A.K.; Kozinski, J.A. Supercritical water gasification of biomass: a state-of-the-art review of process parameters, reaction mechanisms and catalysis. *Sustain. Energy Fuels* **2019**, *3*, 578–598, doi:10.1039/C8SE00565F.
14. Peterson, A.A.; Vogel, F.; Lachance, R.P.; Fröling, M.; Antal, Jr., M.J.; Tester, J.W. Thermochemical biofuel production in hydrothermal media: A review of sub- and supercritical water technologies. *Energy Environ. Sci.* **2008**, *1*, 32, doi:10.1039/b810100k.
15. Vadillo, V.; Sánchez-Oneto, J.; Portela, J.R.; Martínez de la Ossa, E.J. Supercritical Water Oxidation. In *Advanced Oxidation Processes for Waste Water Treatment*; Elsevier, 2018; pp. 333–358 ISBN 9780128105252.
16. Queiroz, A.; Pedroso, G.B.; Kuriyama, S.N.; Fidalgo-Neto, A.A. Subcritical and supercritical water for chemical recycling of plastic waste. *Curr. Opin. Green Sustain. Chem.* **2020**, *25*, 100364, doi:10.1016/j.cogsc.2020.100364.
17. Maxim, F.; Poenaru, I.; Toma, E.E.; Stoian, G.S.; Teodorescu, F.; Hornoiu, C.; Tanasescu, S. Functional Materials for Waste-to-Energy Processes in Supercritical Water. *Energies* **2021**, *14*, 7399, doi:10.3390/en14217399.
18. Peng, G.; Ludwig, C.; Vogel, F. Catalytic supercritical water gasification: Interaction of sulfur with ZnO and the ruthenium catalyst. *Appl. Catal. B Environ.* **2017**, *202*, 262–268, doi:10.1016/j.apcatb.2016.09.011.
19. Xiang, H.; Baudouin, D.; Vogel, F. Metal oxide nanoparticles embedded in porous carbon for sulfur absorption under hydrothermal conditions. *Sci. Rep.* **2023**, *13*, 1–19, doi:10.1038/s41598-023-36395-8.
20. Lane, M.K.M.; Zimmerman, J.B. Controlling metal oxide nanoparticle size and shape with supercritical fluid synthesis. *Green Chem.* 2019, *21*, 3769–3781.
21. Adschiri, T.; Takami, S.; Umetsu, M.; Ohara, S.; Naka, T.; Minami, K.; Hojo, D.; Togashi, T.; Arita, T.; Taguchi, M.; et al. Supercritical Hydrothermal Reactions for Material Synthesis. *Bull. Chem. Soc. Jpn.* **2023**, *96*, 133–147, doi:10.1246/bcsj.20220295.
22. Darr, J.A.; Zhang, J.; Makwana, N.M.; Weng, X. Continuous Hydrothermal Synthesis of Inorganic Nanoparticles: Applications and Future Directions. *Chem. Rev.* **2017**, *117*, 11125–11238, doi:10.1021/acs.chemrev.6b00417.
23. Schwarz, J.A.; Contescu, C.; Contescu, A. Methods for Preparation of Catalytic Materials. *Chem. Rev.* **1995**, *95*, 477–510, doi:10.1021/cr00035a002.
24. Munnik, P.; de Jongh, P.E.; de Jong, K.P. Recent Developments in the Synthesis of Supported Catalysts. *Chem. Rev.* **2015**, *115*, 6687–6718, doi:10.1021/cr500486u.
25. Otsu, J.; Oshima, Y. New approaches to the preparation of metal or metal oxide particles on the surface of porous materials using supercritical water: *J. Supercrit. Fluids* **2005**, *33*, 61–67, doi:10.1016/j.supflu.2004.04.004.

26. Qiu, B.; Han, L.; Wang, J.; Chang, L.; Bao, W. Preparation of Sorbents Loaded on Activated Carbon to Remove H 2 S from Hot Coal Gas by Supercritical Water Impregnation. *Energy & Fuels* **2011**, *25*, 591–595, doi:10.1021/ef101358x.
27. Kumar, K.Y.; Muralidhara, H.B.; Nayaka, Y.A.; Hanumanthappa, H.; Veena, M.S.; Kumar, S.R.K. Hydrothermal Synthesis of Hierarchical Copper Oxide Nanoparticles and its Potential Application as Adsorbent for Pb(II) with High Removal Capacity. *Sep. Sci. Technol.* **2014**, *49*, 2389–2399, doi:10.1080/01496395.2014.922101.
28. Ates, A.; Hatipoglu, H. Evaluation of Stability and Catalytic Activity in Supercritical Water of Zinc Oxide Samples Prepared by the Sol–Gel Method. *J. Inorg. Organomet. Polym. Mater.* **2021**, *31*, 4581–4593, doi:10.1007/s10904-021-02066-2.
29. Fatima, R.; Warsi, M.F.; Zulfiqar, S.; Ragab, S.A.; Shakir, I.; Sarwar, M.I. Nanocrystalline transition metal oxides and their composites with reduced graphene oxide and carbon nanotubes for photocatalytic applications. *Ceram. Int.* **2020**, *46*, 16480–16492, doi:10.1016/j.ceramint.2020.03.213.
30. Farooq, S.; Al Maani, A.H.; Naureen, Z.; Hussain, J.; Siddiqa, A.; Al Harrasi, A. Synthesis and characterization of copper oxide-loaded activated carbon nanocomposite: Adsorption of methylene blue, kinetic, isotherm, and thermodynamic study. *J. Water Process Eng.* **2022**, *47*, 102692, doi:10.1016/j.jwpe.2022.102692.
31. Azam, A.; Ahmed, A.S.; Oves, M.; Khan, M.S.; Memic, A. Size-dependent antimicrobial properties of CuO nanoparticles against Gram-positive and -negative bacterial strains. *Int. J. Nanomedicine* **2012**, *7*, 3527–3535, doi:10.2147/IJN.S29020.
32. Karalis, K.; Ludwig, C.; Niceno, B. Supercritical water anomalies in the vicinity of the Widom line. *Sci. Rep.* **2019**, *9*, 15731, doi:10.1038/s41598-019-51843-0.
33. Ludwig, C.; Casey, W.H. On the Mechanisms of Dissolution of Bunsenite [NiO(s)] and Other Simple Oxide Minerals. *J. Colloid Interface Sci.* **1996**, *178*, 176–185, doi:10.1006/jcis.1996.0106.
34. Barroso-Bogeat, A.; Alexandre-Franco, M.; Fernández-González, C.; Gómez-Serrano, V. Activated carbon surface chemistry: Changes upon impregnation with Al(III), Fe(III) and Zn(II)-metal oxide catalyst precursors from NO3− aqueous solutions. *Arab. J. Chem.* **2019**, *12*, 3963–3976, doi:10.1016/j.arabjc.2016.02.018.
35. Martin, R.B. A stability ruler for metal ion complexes. *J. Chem. Educ.* **1987**, *64*, 402, doi:10.1021/ed064p402.
36. Santoso, S.P.; Angkawijaya, A.E.; Ju, Y.-H. Complex stability in aqueous solution of metal ions (Cu2+, Zn2+, and Mn2+) with pyrocatechuic acid ligand. *Int. J. Adv. Sci. Eng. Technol.* **2015**, *3*, 23–28.
37. Irving, H.; Williams, R.J.P. The stability of transition-metal complexes. *J. Chem. Soc.* **1953**, 3192–3210, doi:10.1039/JR9530003192.
38. Kwon, B.; Liebenberg, L.; Jacobi, A.M.; King, W.P. Heat transfer enhancement of internal laminar flows using additively manufactured static mixers. *Int. J. Heat Mass Transf.* **2019**, *137*, 292–300, doi:10.1016/j.ijheatmasstransfer.2019.03.133.
39. Yoko, A.; Seong, G.; Tomai, T.; Adschiri, T. Continuous flow synthesis of nanoparticles using supercritical water: Process design, surface control, and nanohybrid materials. *KONA Powder Part. J.* **2020**, *37*, 28–41, doi:10.14356/kona.2020002.
40. Demoisson, F.; Ariane, M.; Leybros, A.; Muhr, H.; Bernard, F. Design of a reactor operating in supercritical water conditions using CFD simulations. Examples of synthesized nanomaterials. *J. Supercrit. Fluids* **2011**, *58*, 371–377, doi:10.1016/j.supflu.2011.07.001.

41. Baruah, S.; Dutta, J. Hydrothermal growth of ZnO nanostructures. *Sci. Technol. Adv. Mater.* **2009**, *10*, 013001, doi:10.1088/1468-6996/10/1/013001.
42. Demoisson, F.; Piolet, R.; Ariane, M.; Leybros, A.; Bernard, F. Influence of the pH on the ZnO nanoparticle growth in supercritical water: Experimental and simulation approaches. *J. Supercrit. Fluids* **2014**, *95*, 75–83, doi:10.1016/j.supflu.2014.08.007.